Theoretical and Applied Mechanics Letters 13 (2023) 100463

Contents lists available at ScienceDirect

Theoretical and Applied Mechanics Letters

journal homepage: www.elsevier.com/locate/taml

Full Article

Numerical study of the splashing wave induced by a seaplane using mesh-based and particle-based methods

Yang Xu[a], Peng-Nan Sun[a,*], Xiao-Ting Huang[a], Salvatore Marrone[b], Lei-Ming Geng[c]

[a] School of Ocean Engineering and Technology, Sun Yat-sen University, Zhuhai 519082, China
[b] CNR-INM. Institute of Marine Engineering, Rome 00128, Italy
[c] AVIC General Huanan Aircraft Industry Co., Ltd, Zhuhai 519080, China

ARTICLE INFO

Keywords:
Seaplane
Splashing
Fluid-structure interactions
SPH Method

ABSTRACT

In recent years, forest fires and maritime accidents have occurred frequently, which have had a bad impact on human production and life. Thus, the development of seaplanes is an increasingly urgent demand. It is important to study the taxiing process of seaplanes for the development of seaplanes, which is a strong nonlinear fluid-structure interaction problem. In this paper, the smoothed particle hydrodynamics (SPH) method based on the Lagrangian framework is utilized to simulate the taxiing process of seaplanes, and the SPH results are compared with those of the finite volume method (FVM) based on the Eulerian method. The results show that the SPH method can not only give the same accuracy as the FVM but also have a strong ability to capture the splashing waves in the taxiing process, which is quite meaningful for the subsequent study of the effect of a splash on other parts of the seaplane.

1. Introduction

Seaplanes have shown great application potential in forest fire fighting and maritime rescue. The ability to take off and land on the water surface is the most typical feature of a seaplane, which is different from a roadbed aircraft. Taking off and landing on the water are accompanied by taxiing motion on the water [1]. The water surface environment is different from the land runway. Many factors will affect the performance of the seaplane, which may cause the seaplane to be buried or move like a dolphin. It is very important to study the hydrodynamic performance of the seaplane during the taxiing process for the whole design, and it is also of great significance to the subsequent design of large firefighting/water rescue seaplanes.

At present, the research on the hydrodynamic force of the seaplane during taking-off and landing is mainly divided into model experiments and empirical formulas [2,3]. With the help of some high-precision experimental equipment, physical experiments can capture the splash generated during the taxiing of seaplanes and provide a more practical assessment. However, the scale effect of the model experimental tank and the high experimental cost are unavoidable topics. Recently, due to a huge increase in computing power, a variety of numerical methods have been proposed and applied to the study of the hydrodynamics of water entries [4–7] and taxiing process of seaplanes [8–13]. Among them, the representative one is the Finite Volume Method (FVM). Based on the commercial software FLUENT, Zhao et al. [14] simulated the entire process of seaplane landing on the water surface and captured the change of free surface. In [10], the numerical simulations of the taxiing process of seaplanes at different speeds were carried out based on STAR-CCM+, with overset mesh technology and VOF method, which was consistent with the experimental results.

There are complex fluid movements such as free surface splashing, overturning, and crushing during the taxiing process of seaplanes. The violent splash of the free surface will have a certain impact on the belly and wings of seaplanes, which may cause certain harm to the safety performance of seaplanes. As a class of mesh-free methods based on the Lagrangian view, Smoothed Particle Hydrodynamics (SPH) is very suitable for dealing with free liquid surface tracking [11,15–17], water-gas interface [18], and fluid-structure interface [19–21]. Cheng et al. [16] adopted the SPH model to tackle the ditching problems of a ground-effect wing ship, and some useful conclusions were drawn. Xiao et al. [11] predicted the hydrodynamic behavior of ditching events in terms of hydrodynamic forces, pressure loads, and splashing jet topology by means of an SPH model and analyzed the impact of different initial ditching angles.

As mentioned before, the splashing phenomenon during high-speed taxiing of seaplanes is a fluid-structure interaction problem involving solid-liquid-gas, in which gas also occupies a certain influence. Many scholars have studied the behavior of gas, especially the bubble in the fluid [22]. Zhang and Ni [23] accurately simulated the behaviors of the entrained bubble in complex flows and discovered the influence mech-

* Corresponding author.
E-mail address: sunpn@mail.sysu.edu.cn (P.-N. Sun).

https://doi.org/10.1016/j.taml.2023.100463
Received 17 June 2023; Received in revised form 21 June 2023; Accepted 27 June 2023
Available online 5 July 2023

anism of fluid properties on the bubble dynamics, which provided good guidance for the research of complex water-gas multiphase flows. At present, the research focus of this paper is on seaplanes and water, and the influence of air will be considered in subsequent research.

In this work, based on the SPH method and the FVM method, the process of seaplane taxiing on the still water surface is simulated. The feasibility of the SPH method to simulate the taxiing process of the seaplane is analyzed and its ability to capture free surface splash is emphasized.

2. Numerical methods

2.1. Governing equation

The solution to fluid dynamics problems is mainly based on a system of partial differential equations for the fields of variables such as density, velocity, and energy. In this paper, the system of SPH theory under the weakly compressible assumption will be described in terms of the basic governing equations. The governing equations [24] for a positive pressure fluid based on the weakly compressible assumption are as follows

$$\begin{cases} \frac{\mathrm{D}\rho}{\mathrm{D}t} = -\rho\nabla\cdot\boldsymbol{u}, \\ \frac{\mathrm{D}\boldsymbol{u}}{\mathrm{D}t} = \frac{\nabla\cdot\boldsymbol{T}}{\rho} + \boldsymbol{g}, \\ \frac{\mathrm{D}\boldsymbol{r}}{\mathrm{D}t} = \boldsymbol{u}, \\ p = {c_0}^2\left(\rho-\rho_0\right), \end{cases} \tag{1}$$

where $\frac{\mathrm{D}}{\mathrm{D}t}$ is the material derivative concerning time or the Lagrangian derivative. ρ, $\boldsymbol{u}$, $\boldsymbol{r}$ denote the density, velocity, and position vector of the fluid, respectively. $\boldsymbol{g}$ is the acceleration of gravity. $\boldsymbol{T}$ is the stress tensor of a Newtonian fluid. To solve the above governing equations in the SPH framework, these equations need to be discretized by particles.

2.2. SPH discretization of governing equations

In the SPH framework, the computational domain is discretized into particles carrying physical properties such as density, pressure, velocity, etc. [25]. The SPH equation is constructed in two steps, the first being the continuous integral representation, also known as the kernel approximation. The continues integral representation of a field function $f(\boldsymbol{r})$ [24] is

$$\begin{cases} f(\boldsymbol{r}) \approx \langle f(\boldsymbol{r})\rangle = \int_\Omega f\left(\boldsymbol{r}'\right)W\left(\boldsymbol{r}-\boldsymbol{r}',h\right)\mathrm{d}\boldsymbol{r}', \\ \nabla_r f(\boldsymbol{r}) \approx \langle \nabla_r f(\boldsymbol{r})\rangle = \int_\Omega f\left(\boldsymbol{r}'\right)\nabla_r W\left(\boldsymbol{r}-\boldsymbol{r}',h\right)\mathrm{d}\boldsymbol{r}', \end{cases} \tag{2}$$

where W is the kernel function. Since the Wendland C2 kernel function has many excellent features, it is selected as the kernel function here. ∇_r represents the gradient of relative position $\boldsymbol{r}$, and h denotes the smoothing length. The next thing to do is particle approximation [24], turning the continuity integral into a discrete sum of particles as follows

$$\begin{cases} f\left(\boldsymbol{r}_i\right) = \sum_j f\left(\boldsymbol{r}_j\right)W\left(\boldsymbol{r}_i-\boldsymbol{r}_j,h_i\right)V_j, \\ \nabla_i f\left(\boldsymbol{r}_i\right) = \sum_j \left[f\left(\boldsymbol{r}_j\right)+f\left(\boldsymbol{r}_j\right)\right]\nabla W\left(\boldsymbol{r}_i-\boldsymbol{r}_j,h_i\right)V_j, \\ \nabla_i\cdot\boldsymbol{f}\left(\boldsymbol{r}_i\right) = \sum_j \left[\boldsymbol{f}\left(\boldsymbol{r}_j\right)-\boldsymbol{f}\left(\boldsymbol{r}_j\right)\right]\cdot\nabla_i W\left(\boldsymbol{r}_i-\boldsymbol{r}_j,h_i\right)V_j. \end{cases} \tag{3}$$

In the above equation, the subscripts i, j are the particle numbers; j represents any other particle number in the tightly-branched domain of the particle i. V_j represents the volume of the particle j and can be obtained from its mass and density. The Eq. (3) shows the particle approximation of the function and its gradient and divergence.

2.3. δ-SPH model

In this study, the δ-SPH model [26,27] is adopted, which is used widely in the SPH community. Its accuracy and robustness in simulating fluid-solid interaction problems, especially when it involves large deformation of the water surface, meet the calculation requirements. The governing equations [28] are derived as follows

$$\begin{cases} \frac{\mathrm{D}\rho_i}{\mathrm{D}t} = -\rho_i\sum_j\left(\boldsymbol{u}_j-\boldsymbol{u}_i\right)\cdot\nabla_i W_{ij}V_j + \mathcal{T}_i^{(D)}, \\ \frac{\mathrm{D}\boldsymbol{u}_i}{\mathrm{D}t} = -\frac{1}{\rho_i}\sum_j\left(p_i+p_j\right)\nabla_i W_{ij}V_j + \boldsymbol{g} + \mathcal{T}_i^{(V)}, \\ \frac{\mathrm{D}\boldsymbol{r}_i}{\mathrm{D}t} = \boldsymbol{u}_i\ , \quad V_i(t) = \frac{m_i}{\rho_i(t)}, \\ p_i = c_0^2\left(\rho_i-\rho_0\right), \end{cases} \tag{4}$$

where p is the pressure. The density diffusive term, introduced in the continuity equation, as the most critical superiority of the δ-SPH model, can remove the pressure noise efficiently, which is written as $\mathcal{T}_i^{(D)}$ in Eq. (4). $\mathcal{T}_i^{(D)}$ is given in detail as

$$\begin{cases} \mathcal{T}_i^{(D)} = \delta c_0 h_i\sum_j \pi_{ij}\cdot\nabla_i W_{ij}V_j, \\ \pi_{ij} = 2\left(\rho_j-\rho_i\right)\frac{\boldsymbol{r}_j-\boldsymbol{r}_i}{\|\boldsymbol{r}_j-\boldsymbol{r}_i\|^2} - \left[\langle\nabla\rho\rangle_i^L + \langle\nabla\rho\rangle_j^L\right], \end{cases} \tag{5}$$

where the coefficient δ is usually adopted as 0.1 and $\langle\nabla\rho\rangle^L$ represents the renormalized density gradient [29]. Moreover, an artificial viscosity term $\mathcal{T}_i^{(V)}$ [28] is taken into the momentum equation to guarantee numerical stability, which is given as

$$\begin{cases} \mathcal{T}_i^{(V)} = \frac{\alpha c_0 h_i\rho_0}{\rho_i}\sum_j \Pi_{ij}\nabla_i W_{ij}V_j\ , \\ \Pi_{ij} = \frac{\left(\boldsymbol{u}_j-\boldsymbol{u}_i\right)\cdot\left(\boldsymbol{r}_j-\boldsymbol{r}_i\right)}{\|\boldsymbol{r}_j-\boldsymbol{r}_i\|^2+0.01h_i^2}\ , \end{cases} \tag{6}$$

where α is set to 0.02. In order to solve the above governing equation, it is also necessary to decouple density ρ and pressure p, which is implemented here using the linearized Tait *Equation of State* (EoS). It means the pressure directly depends on the reference density seeing the last line in Eq. (4), where c_0 represents the initial artificial speed of sound and ρ_0 represents the initial fluid density. In the WCSPH framework, the value of c_0, according to the limitation of Mach number [30], should guarantee that

$$c_0 \geq 10\max\left(U_{\max}, \sqrt{\frac{P_{\max}}{\rho_0}}\right), \tag{7}$$

where $U_{\max}$ and $P_{\max}$ stand for the maximum anticipated fluid velocity and pressure during the SPH simulation, respectively.

2.4. Multi-resolution technology

In order to improve the computational accuracy and reduce the total computational cost, the technique of adaptive particle refinement (hereafter shortened to APR) [31–33] is imposed in this paper. This technique is inspired by the adaptive mesh refinement (AMR) developed in mesh-based models. Particles of different resolutions are defined as different sets of particles, denoted by $level(k)$ where k represents the level of particle resolution. For example, the particles of the initial layer belong to $level(0)$. The particle splitting occurs when the particles enter the refinement region. In the three-dimensional problem, a parent particle ($level(k)$) splits into eight sub-particles (the splitting process is shown in Fig. 2). During the splitting process, the initial particles are still retained, and a new set of particles is generated as $level(k+1)$. The particles of the layer $level(k)$ are called parent particles, while the particles of the layer $level(k+1)$ are child particles (shown in Fig. 2). Importantly, during the SPH simulation, the parent particles are turned off as inactive, i.e., they no longer participate in the SPH simulation but still update particle information and follow the flow field motion by interpolating the data from the daughter particles within the support domain. The daughter particle formed by the splitting is active and begins to participate in the flow field calculation. Arbitrary physical represents ϕ (e.g., pressure, velocity and density) for inactive particles can be interpolated from the surrounding SPH particles using the Shepard interpolation method [34] with the following equation

$$\phi_i = \sum_{j\in\mathrm{SPH}}\phi_j W_{ij} \Big/ \sum_{j\in\mathrm{SPH}} W_{ij}\ . \tag{8}$$

Fig. 1. The seaphane of "AG600". Photo from AVIC GA Huanan Aircraft Industry Co., Ltd .

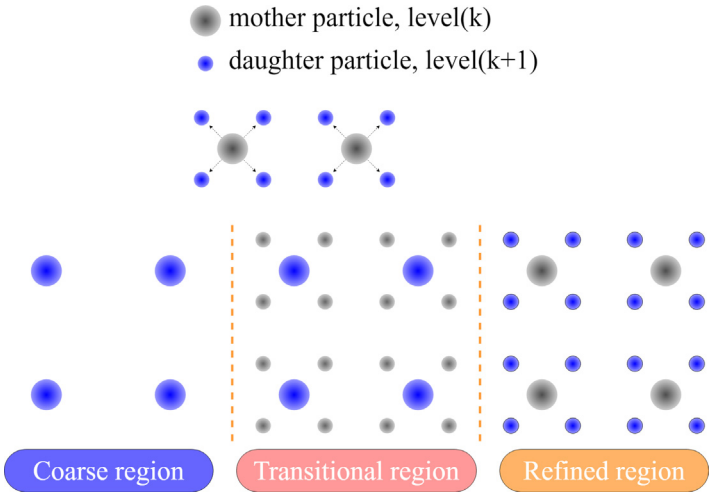

Fig. 2. Schematic diagram of adaptive particle refinement.

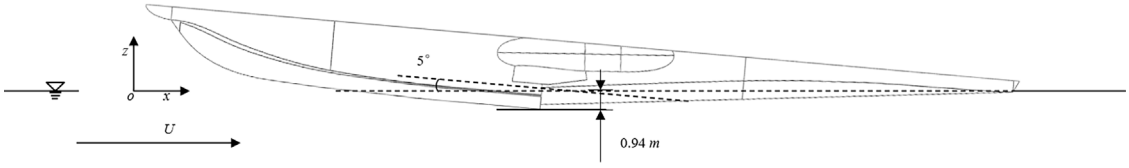

Fig. 3. The initial state of the seaplane (with a 5-degree angle to the water surface).

It is also specified that particles in every layer only interact with particles in the same layer, which means that at the edge of $level(k+1)$, a transition region needs to be extended (as shown in Fig. 2) with a width greater than the radius of the kernel function in layer $level(k+1)$, for the sake of preventing errors due to truncation of the kernel function. In the transition region, the active and inactive characteristics of the particles are completely opposite to the refinement region In particular, when the inactive parent particles are out of the particle refinement region, they are reactivated and become SPH particles and then participate in the SPH calculation normally, while the refined daughter particles flow out of the refinement region and its transition region. The principle and implementation of multi-level resolution are introduced in detail above, through which the multi-level resolution model can be implemented in the SPH model to improve the local calculation accuracy.

3. Numerical simulation and comparative analysis

3.1. Model parameters

In order to reduce computing resources, parts of the seaplane in contact with water are taken into consideration, and other accessories, such as wings, are not considered. The model is shown in Fig. 3. The origin of the coordinate is located at the intersection of the longitudinal section of the seaplane and the still water surface. The x-axis direction points to the tail of the seaplane, and the z-axis direction is vertically upward. In the numerical simulation, the seaplane is fixed, and the taxiing process is realized by employing uniform incoming flow.

As the world's largest seaplane in development, AG600 (shown in Fig. 1) has a length of 36.9 m and a height of 12.1 m. Its external size is comparable to that of the Boeing 737. The maximum load capacity reaches 12 tons, and the taking-off speed reaches 300 km/h, which is higher than any other high-speed ship in the world.

In this paper, an in-house SPH program and commercial software STAR-CCM+ based on FVM are used to simulate different working conditions, respectively, and the results of the two are compared. To compare the results more credible, two different speeds are set up, 30 m/s and 80 m/s.

The APR is utilized to improve accuracy and reduce the total calculation time and cost. A smaller particle spacing is set near the seaplane to capture the change of the free surface. A larger particle spacing is set in the part away from the seaplane to reduce the number of particles in the computational domain and improve computational efficiency. Figure 4 shows the initial state of SPH simulation. Correspondingly, the

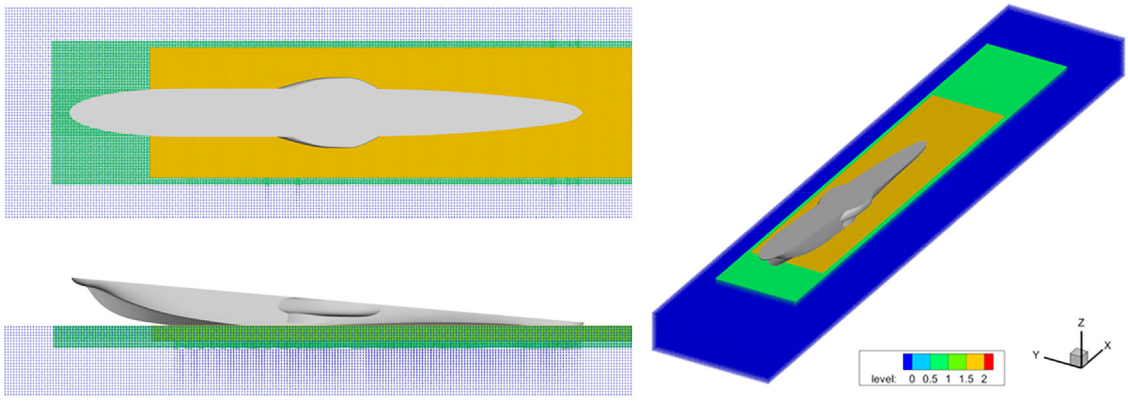

Fig. 4. Configuration of seaplane taxiing with high speed simulated with SPH methods combined with APR. On the left, from top to bottom, the top view and side view are given, respectively, and the right is a full view of the simulation tank.

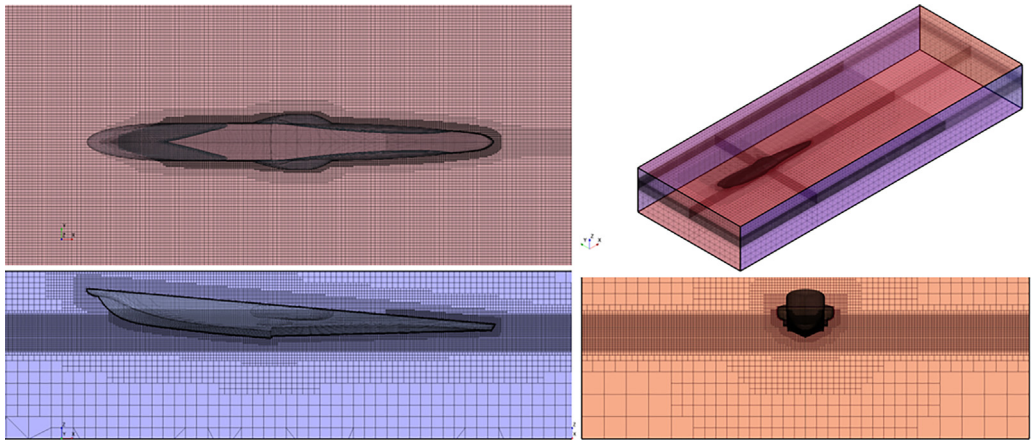

Fig. 5. Configuration of seaplane taxiing with high speed simulated with FVM methods with refined mesh. On the left, from top to bottom, the top view and side view are given, respectively, while the right is a full view and front view of the simulation tank.

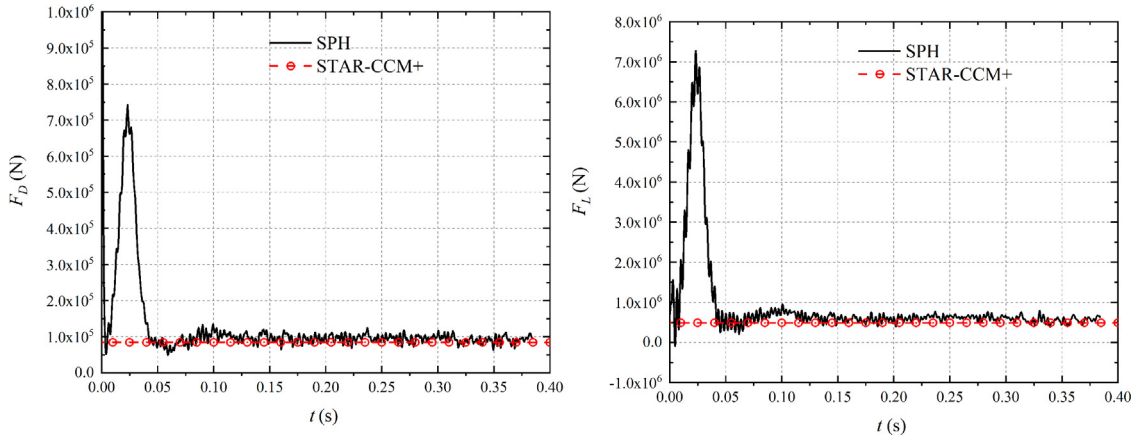

Fig. 6. The SPH results of drag and lift force validated with FVM results with a speed of 30 m/s.

numerical tank is established, and the numerical simulation of the taxiing process of the seaplane at different speeds is carried out, combined with VOF, to capture the free surface. The calculation domain length and grid settings in STAR-CCM+ are shown in Fig. 5 below. The boundary layer setting has a great impact on fluid simulation, and for large-scale high-speed taxiing, the Y+ setting of less than 100 can meet the requirements of free surface simulation. Similar to the operation in SPH simulation, the computational domain is divided into different regions, and the mesh size of the region where the free surface changes greatly are refined.

Convergence analysis is necessary before a numerical study. In the SPH and FVM simulations, since multi-resolution techniques (APR for SPH and AMR for FVM) can be applied, the flow details can be well resolved close to the structure. After a convergence analysis, we adopted the particle/mesh refinement strategy as follows. Two refinement operations are performed in the SPH simulation. The initial particle spacing is 0.2 m, and in the area near the seaplane, the particle spacing is refined to 0.05 m. In the FVM simulation, considering the free surface, the mesh sizes of x, y, and z along the three directions of the coordinate axis are set to 0.0625 m, 0.0625 m, and 0.0625 m, respectively. The

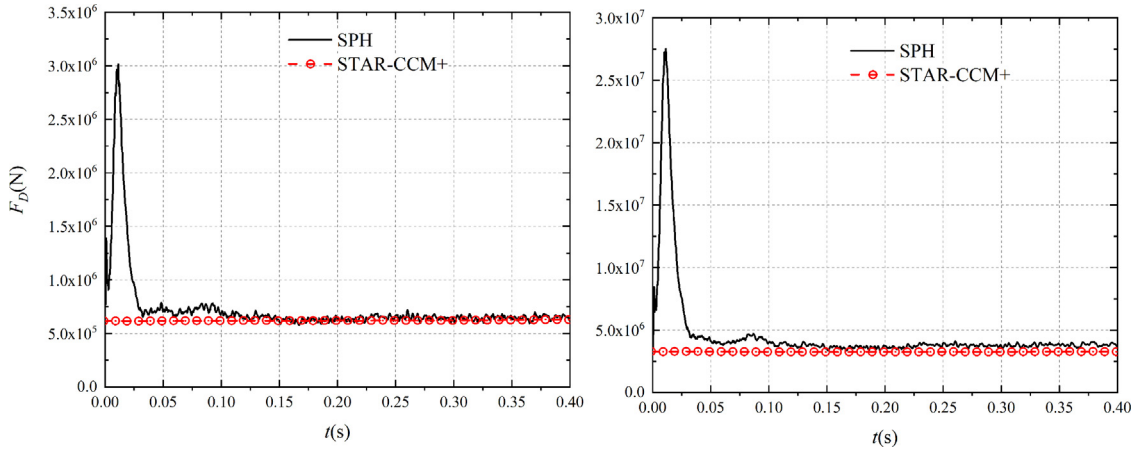

Fig. 7. The SPH results of drag and lift force validated with FVM results with a speed of 80 m/s.

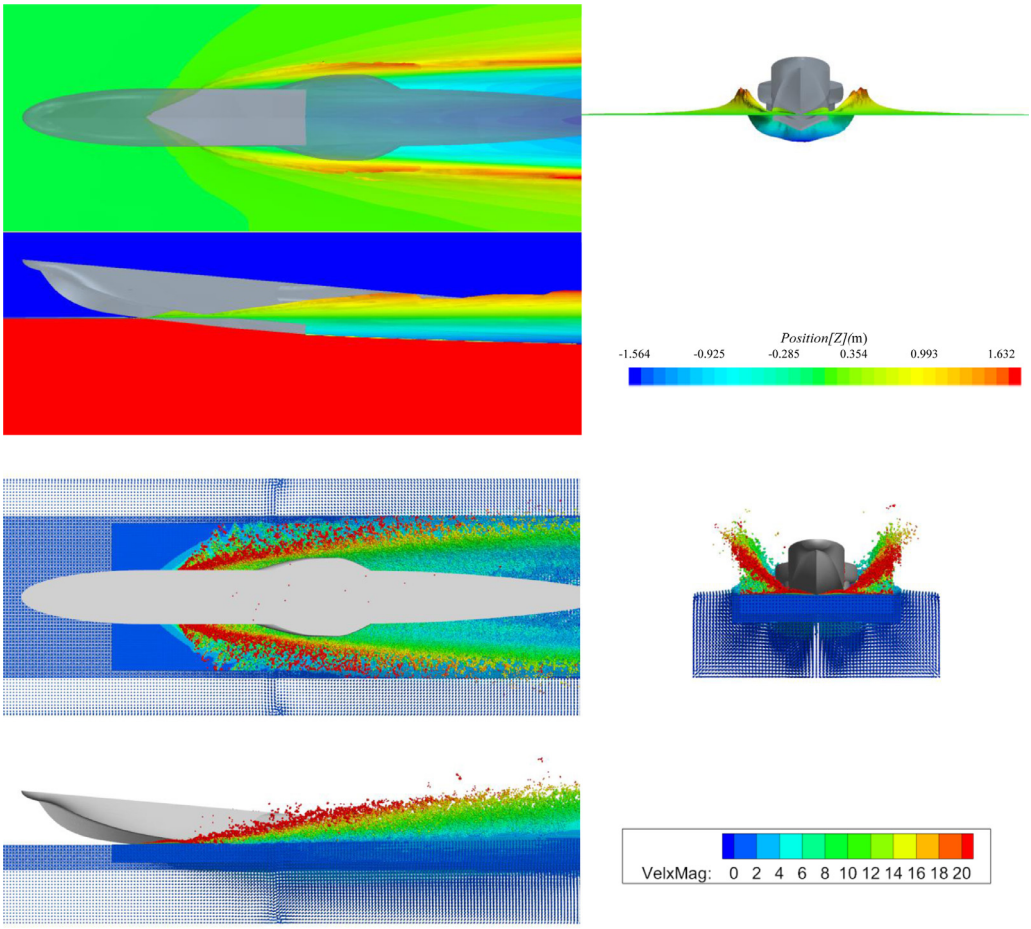

Fig. 8. The comparison of the splashing of free-surface between (top) FVM and (bottom) SPH results.

total number of particles required for the numerical simulation of the SPH method is around 6.85 million, and the number of grids for FVM is about 7.42 million.

3.2. Comparative analysis of drag and lift

Figures 6 and 7 show the lift and drag results obtained by the SPH method and FVM at two different speeds. From a macroscopic point of view, the results of the two are very close, and the results of the SPH method reach an accuracy comparable to the commercial software. This shows that the SPH method used in this paper can be applied to calculate the lift and drag of the seaplane during the taxiing process, and the results are reliable.

In this paper, the taxiing speed of two seaplanes is numerically simulated, and the calculation results of lift and drag at different speeds are compared and analyzed. Thanks to the special structure design of the water part of the seaplane, the lift force is greater than the drag force at high speed, whether 30 m/s or 80 m/s, which is very beneficial to the subsequent taking-off process of the seaplane. As the taxiing speed increases, the lift and drag of the seaplane increase.

Analyzing the result in more detail, the resistance obtained by the SPH method will be slightly greater than the results of FVM. One possi-

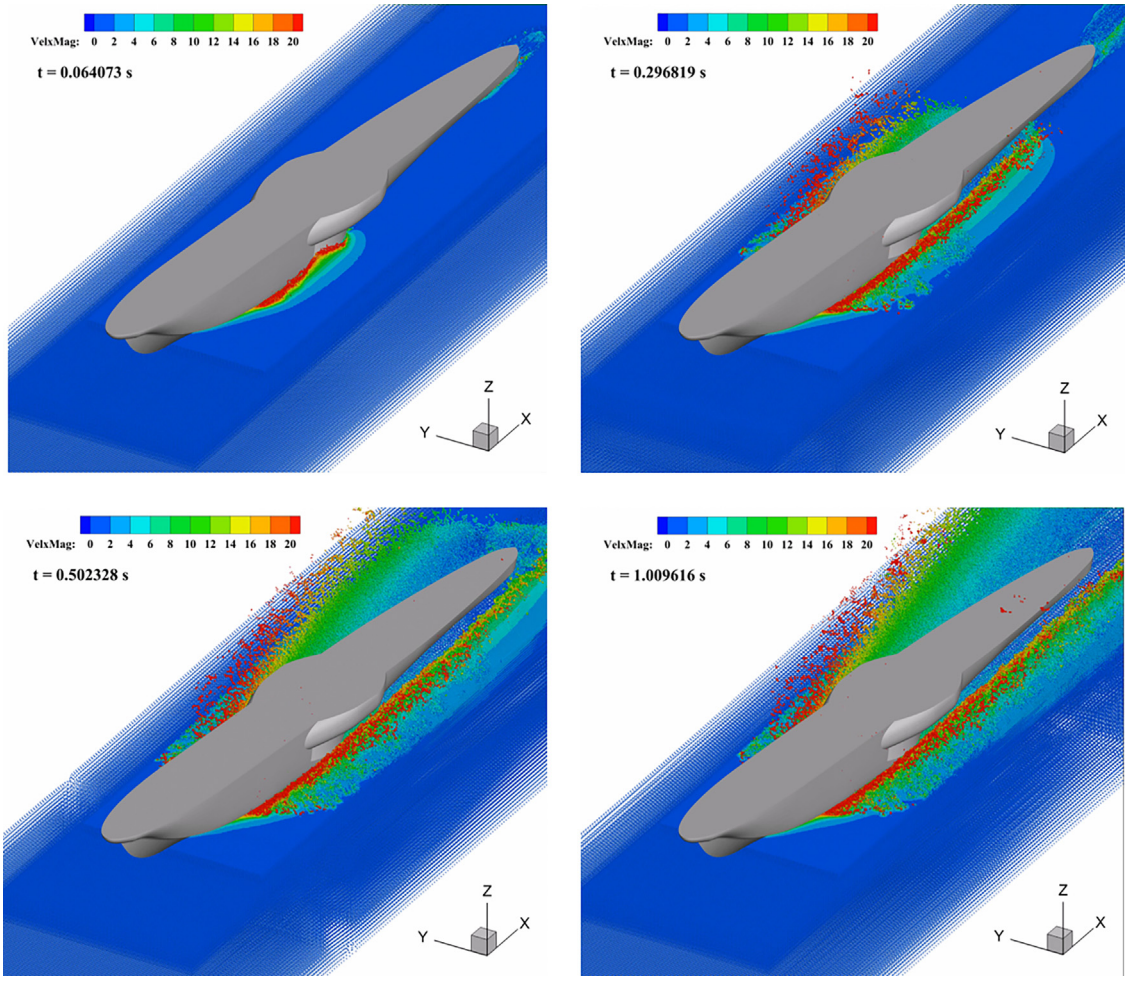

Fig. 9. Splashing of the flow field at different time instants.

ble reason is that the surrounding fluid splashes during high-speed taxiing, and the splashing fluid slams the seaplane. The SPH method has a strong ability to capture these splashes, and the slamming pressure generated by the splash increases the resistance of the seaplane, which is also consistent with the results of the model test [10]. The splashing phenomenon in the taxiing process is discussed in more detail in the next section.

3.3. Splash characteristics of flow field

In the process of high-speed taxiing of seaplane, the splash of the free surface is inevitable. Figure 8 shows the simulation results of FVM when the seaplane taxis at a high speed of 80 m/s. The separation of the fluid and the seaplane surface and the splash phenomenon can be found in the first part of the seaplane. The splash continues to develop to the tail of the aircraft, and finally, the seaplane forms a stable Kelvin wave on the water's surface.

Figure 8 shows the splash results of three different perspectives of the seaplane at a speed of 80 m/s calculated by the in-house SPH program. To clearly show the splash effect, the speed is processed, the parameter VelxMax is set, and the calculation method is $\mathrm{VelxMag} = \sqrt{((u_x - 80)^2 + u_y^2 + u_z^2)}$. Comparing the position of the splash, it can be found that the results of SPH and FVM are consistent, both of which are generated at the head and develop to the tail. However, there are certain differences in the wave surface and tail waveforms around the seaplane model at different speeds. For example, at high speeds (80 m/s), the width of the tail Kelvin wave is small.

The difference is that the SPH method captures more obvious free surface splashes and flips, the width of the Kelvin wave of SPH is bigger, and the height of the splash calculated by the SPH method is significantly higher than the result of FVM. The splash state of the seaplane during high-speed taxiing calculated by the SPH method is shown in Fig. 9.

Limited by the grid, it is difficult for FVM to simulate the real form of a splash when the seaplane is taxiing at high speed. As a meshless method of the pure Lagrangian framework, the SPH method has a natural advantage in describing violent fluid deformations. In addition, thanks to the omission of the convection term in the control equation, numerical diffusion is prevented at the interfaces when simulating high-speed flows. For the splash phenomenon of seaplane taxiing studied in this paper, the SPH method can not only reach the same calculation accuracy comparable to the commercial software but also capture the splash phenomenon well, which is of great significance for the next step to study the influence of splash on other components of the seaplane.

4. Conclusions

In this paper, the splash problem caused by high-speed taxiing of seaplanes is studied. SPH (particle-based method) and FVM (mesh-based method) are utilized to simulate it, respectively. A numerical tank is established in FVM, and the VOF method is used to capture the change of the free surface so as to realize the numerical simulation of the splash problem. The free surface condition of the SPH method is automatically satisfied at the free surface, and no special treatment is needed. In order to improve the accuracy and reduce the total calculation time, Adaptive Particle Refinement is utilized. The drag force, lift force, and splash

characteristics of a seaplane taxiing at two speeds are numerically studied. At a larger taxiing speed, a larger splash of the free surface occurs around the seaplane. Compared with the FVM calculation results, the lift and drag results of SPH calculation have a small deviation within the allowable error range, which indicates that the load prediction by the SPH method for the seaplane taxiing process is reliable. Compared with the free surface splash calculated by FVM, it is shown that the SPH method can better capture the splash phenomenon during the high-speed taxiing of the seaplane, which is of great significance for the next study of the impact of a splash on other components of the seaplane. In summary, the SPH method can obtain similar accuracy with respect to FVM in terms of the overall hydrodynamic force calculation, but the height of the splashing wave obtained by SPH is higher than that of FVM, which is closer to real physical phenomena. Compared to FVM, the computational efficiency of SPH should be further improved. In future studies, the SPH simulation can be accelerated with GPU (graphics processing unit) parallel computing. On the other hand, a coupling technique between SPH and FVM can be developed. The research conclusions of this paper can provide a reference and basis for the anti-spatter design of seaplanes. To a certain extent, it is expected to greatly shorten the development cycle of seaplanes and improve water taxiing performance.

Declaration of Competing Interest

The authors declare that they have no known competing financial interests or personal relationships that could have appeared to influence the work reported in this paper.

CRediT authorship contribution statement

Yang Xu: Formal analysis, Validation, Investigation, Visualization, Writing – original draft. **Peng-Nan Sun:** Conceptualization, Methodology, Software, Resources, Data curation, Supervision, Funding acquisition, Project administration, Writing – review & editing. **Xiao-Ting Huang:** Visualization, Writing – review & editing. **Salvatore Marrone:** Writing – review & editing. **Lei-Ming Geng:** Writing – review & editing.

Acknowledgments

This research was supported by: the National Key Research and Development Program of China (Grant No. 2021YFC2800700); the National Natural Science Foundation of China (Grant Nos. 52171329 and 12002404); the Natural Science Foundation of Guangdong Province of China (Grant No. 2022A1515012084); and the Fundamental Research Funds for the Central Universities, Sun Yat-sen University (Grant No. 231gbi023). This work was also supported by the GHfund A (Grant No. ghfund202302014084).

The OceanConnect High-Performance Computing Cluster of Sun Yat-sen University that supports scientific computing in this paper is also acknowledged.

References

[1] A.L. Canamar Leyva, Seaplane conceptual design and sizing, University of Glasgow, 2012 MSc(R). https://eleanor.lib.gla.ac.uk/record=b2969080

[2] T. von Kármán, The impact on seaplane floats during landing, 1929, Num Pages: 9 Place: Washington, DC Publisher: National Advisory Committee on Aeronautics, https://resolver.caltech.edu/CaltechAUTHORS:20140804-120956389.

[3] X. Zheng, B. Wu, M. Wang, B. Tang, Experiment and simulation on clam water taxiing of seaplane based on CFD, J. Phys. Conf. Ser. 1300 (1) (2019) 012041, doi:10.1088/1742-6596/1300/1/012041.

[4] S.-Y. Zhong, P.-N. Sun, Y.-X. Peng, N.-N. Liu, H.-G. Lyu, X.-T. Huang, An SPH study of slamming and splashing at the bow of SYSU vessel, Ocean Eng. 269 (2023) 113581, doi:10.1016/j.oceaneng.2022.113581.

[5] X. Huang, P. Sun, H. Lyu, A.-M. Zhang, Water entry problems simulated by an axisymmetric SPH model with VAS scheme, J. Mar. Sci. Appl. 21 (2) (2022) 1–15, doi:10.1007/s11804-022-00265-y.

[6] W.-T. Liu, A.-M. Zhang, X.-H. Miao, F.-R. Ming, Y.-L. Liu, Investigation of hydrodynamics of water impact and tail slamming of high-speed water entry with a novel immersed boundary method, J Fluid Mech 958 (2023) A42, doi:10.1017/jfm.2023.120. Publisher: Cambridge University Press

[7] P.N. Sun, C. Pilloton, M. Antuono, A. Colagrossi, Inclusion of an acoustic damper term in weakly-compressible SPH models, J Comput Phys 483 (2023) 112056, doi:10.1016/j.jcp.2023.112056.

[8] T. Xiao, N. Qin, Z. Lu, X. Sun, M. Tong, Z. Wang, Development of a smoothed particle hydrodynamics method and its application to aircraft ditching simulations, Aerosp. Sci. Technol. 66 (2017) 28–43, doi:10.1016/j.ast.2017.02.022.

[9] X. Duan, W. Sun, C. Chen, M. Wei, Y. Yang, Numerical investigation of the porpoising motion of a seaplane planing on water with high speeds, Aerosp. Sci. Technol. 84 (2019) 980–994, doi:10.1016/j.ast.2018.11.037.

[10] X. Zheng, S. Quan, B. Wu, X. Han, Numerical simulation of seaplane water takeoff process based on CFD, J. Phys. Conf. Ser. 2030 (1) (2021) 012103, doi:10.1088/1742-6596/2030/1/012103.

[11] T. Xiao, Z. Lu, S. Deng, Effect of initial pitching angle on helicopter ditching characteristics using smoothed-particle-hydrodynamics method, J Aircr 58 (1) (2021) 167–181, doi:10.2514/1.C035898.

[12] J. Chen, T. Xiao, M. Wang, Y. Lu, M. Tong, Numerical study of wave effect on aircraft water-landing performance, Applied Sciences 12 (5) (2022) 2561, doi:10.3390/app12052561.

[13] Q. Wen, Z. Cheng, R. Deng, K. Yang, Influence of wave parameters on taxiing characteristics of seaplane, in: W. Fan, L. Zhang, N. Li, X. Song (Eds.), Methods and Applications for Modeling and Simulation of Complex Systems, Communications in Computer and Information Science, Springer Nature, Singapore, 2022, pp. 347–358, doi:10.1007/978-981-19-9198-1_26.

[14] Y. Zhao, Q. Qu, P. Liu, Numerical study on mechanical properties of seaplane in whole water surface landing process, Journal of Beijing University of Aeronautics and Astronautics 46 (4) (2020) 830–838, doi:10.13700/j.bh.1001-5965.2019.0462.

[15] A.-m. Zhang, P.-n. Sun, F.-r. Ming, A. Colagrossi, Smoothed particle hydrodynamics and its applications in fluid-structure interactions, Journal of Hydrodynamics, Ser. B 29 (2) (2017) 187–216, doi:10.1016/S1001-6058(16)60730-8.

[16] H. Cheng, F.R. Ming, P.N. Sun, P.P. Wang, A.M. Zhang, Towards the modeling of the ditching of a ground-effect wing ship within the framework of the SPH method, Appl. Ocean Res. 82 (2019) 370–384, doi:10.1016/j.apor.2018.09.014.

[17] A. Di Mascio, S. Marrone, A. Colagrossi, L. Chiron, D. Le Touzé, SPH-FV coupling algorithm for solving multi-scale three-dimensional free-surface flows, Appl. Ocean Res. 115 (2021) 102846, doi:10.1016/j.apor.2021.102846.

[18] P. Sun, A.-M. Zhang, S. Marrone, F. Ming, An accurate and efficient SPH modeling of the water entry of circular cylinders, Appl. Ocean Res. 72 (2018) 60–75, doi:10.1016/j.apor.2018.01.004.

[19] A. Khayyer, H. Gotoh, H. Falahaty, Y. Shimizu, An enhanced ISPH-SPH coupled method for simulation of incompressible fluid-elastic structure interactions, Comput Phys Commun 232 (2018) 139–164, doi:10.1016/j.cpc.2018.05.012.

[20] S. Marrone, A. Colagrossi, L. Chiron, M. De Leffe, D. Le Touzé, High-speed water impacts of flat plates in different ditching configuration through a Riemann-ALE SPH model, Journal of Hydrodynamics 30 (1) (2018) 38–48, doi:10.1007/s42241-018-0004-y.

[21] X.-Y. Ju, P.-N. Sun, Y.-M. Shen, J.-Q. Chen, A.-M. Zhang, Study on the ditching of space capsules using the smoothed particle hydrodynamics method, Ocean Eng. 281 (2023) 114714, doi:10.1016/j.oceaneng.2023.114714.

[22] A.-M. Zhang, S.-M. Li, P. Cui, S. Li, Y.-L. Liu, A unified theory for bubble dynamics, Physics of Fluids 35 (3) (2023) 033323, doi:10.1063/5.0145415.

[23] A.-M. Zhang, B.-Y. Ni, Influences of different forces on the bubble entrainment into a stationary Gaussian vortex, Science China Physics, Mechanics and Astronomy 56 (11) (2013) 2162–2169, doi:10.1007/s11433-013-5267-2.

[24] G.-R. Liu, M.B. Liu, Smoothed Particle Hydrodynamics: A Meshfree Particle Method, World Scientific, 2003. Google-Books-ID: _cwFMmEQvZQC

[25] M.B. Liu, G.R. Liu, Smoothed particle hydrodynamics (sph): an overview andärecent developments, Arch. Comput. Methods Eng. 17 (1) (2010) 25–76, doi:10.1007/s11831-010-9040-7. Identifier: 9040

[26] P. Sun, F. Ming, A. Zhang, Numerical simulation of interactions between free surface and rigid body using a robust SPH method, Ocean Eng. 98 (2015) 32–49, doi:10.1016/j.oceaneng.2015.01.019.

[27] P.-N. Sun, D. Le Touzé, G. Oger, A.-M. Zhang, An accurate FSI-SPH modeling of challenging fluid-structure interaction problems in two and three dimensions, Ocean Eng. 221 (2021) 108552, doi:10.1016/j.oceaneng.2020.108552.

[28] S. Marrone, M. Antuono, A. Colagrossi, G. Colicchio, D. Le Touzé, G. Graziani, δ-SPH model for simulating violent impact flows, Comput Methods Appl Mech Eng 200 (13) (2011) 1526–1542, doi:10.1016/j.cma.2010.12.016.

[29] M. Antuono, A. Colagrossi, S. Marrone, D. Molteni, Free-surface flows solved by means of SPH schemes with numerical diffusive terms, Comput Phys Commun 181 (3) (2010) 532–549, doi:10.1016/j.cpc.2009.11.002.

[30] M. Antuono, S. Marrone, A. Colagrossi, B. Bouscasse, Energy balance in the δ-SPH scheme, Comput Methods Appl Mech Eng 289 (2015) 209–226, doi:10.1016/j.cma.2015.02.004.

[31] L. Chiron, G. Oger, M. de Leffe, D. Le Touzé, Analysis and improvements of adaptive particle refinement (APR) through CPU time, accuracy and robustness considerations, J Comput Phys 354 (2018) 552–575, doi:10.1016/j.jcp.2017.10.041.

[32] P. Sun, A. Colagrossi, S. Marrone, M. Antuono, A. Zhang, Multi-resolution delta-plus-SPH with tensile instability control: towards high Reynolds number flows, Comput Phys Commun 224 (2018) 63–80, doi:10.1016/j.cpc.2017.11.016.

[33] H.-G. Lyu, P.-N. Sun, J.-M. Miao, A.-M. Zhang, 3D multi-resolution SPH modeling of the water entry dynamics of free-fall lifeboats, Ocean Eng. 257 (2022) 111648, doi:10.1016/j.oceaneng.2022.111648.

[34] D. Shepard, A two-dimensional interpolation function for irregularly-spaced data, in: Proceedings of the 1968 23rd ACM national conference, in: ACM '68, Association for Computing Machinery, New York, NY, USA, 1968, pp. 517–524, doi:10.1145/800186.810616.